Hindawi Publishing Corporation
Journal of Nanomaterials
Volume 2016, Article ID 6272983, 17 pages
http://dx.doi.org/10.1155/2016/6272983

Research Article

A Novel Hierarchical Structured Poly(lactic acid)/Titania Fibrous Membrane with Excellent Antibacterial Activity and Air Filtration Performance

Zhe Wang,[1] Zhijuan Pan,[1,2] Jigen Wang,[3] and Ruizhi Zhao[3]

[1]*College of Textile and Clothing Engineering, Soochow University, Suzhou 215123, China*
[2]*National Engineering Laboratory for Modern Silk, Suzhou 215123, China*
[3]*Jiangsu Dasheng Group Co. Ltd., Jiangsu, Nantong 226002, China*

Correspondence should be addressed to Zhijuan Pan; zhjpan@suda.edu.cn

Received 25 October 2015; Accepted 14 January 2016

Academic Editor: Jin-Ho Choy

Hybrid poly(lactic acid)/titania (PLA/TiO_2) fibrous membranes exhibiting excellent air filtration performance and good antibacterial activity were prepared via the electrospinning technique. By varying the composition of the precursor solutions and the relative humidity, the morphologies of PLA/TiO_2 fibers, including the nanopores and nanometer-scale protrusions on the surface of the fibers, could be regulated. The distribution of nanopores and TiO_2 nanoparticles on the surface of PLA/TiO_2 fibers was investigated. Nitrogen adsorption-desorption analysis revealed that nanopores and nanometer-scale protrusions play an important role in improving the specific surface area and nanopore volume of the relevant PLA/TiO_2 fibrous membrane. Filtration performance tests conducted by measuring the penetration of sodium chloride aerosol particles with a 260 nm mass median diameter indicated that fibers with a high surface roughness, large specific surface area, and large nanopore volume greatly improved the particle capture efficiency and facilitated the penetration of airflow. Furthermore, the introduction of TiO_2 nanoparticles endows the relevant fibrous membrane with antibacterial properties. The as-prepared PLA/TiO_2 fibrous membrane loaded with 1.75 wt% TiO_2 nanoparticles formed at a relative humidity of 45% exhibited a high filtration efficiency (99.996%) and a relatively low pressure drop (128.7 Pa), as well as a high antibacterial activity of 99.5%.

1. Introduction

Particulate matter pollution has drawn increasing attention because it may cause serious health problems, such as respiratory diseases, cardiovascular illness, and allergies [1–3]. Suspended particles with diameters smaller than 2.5 μm were considered particularly harmful because they can penetrate human bronchi, lungs, and even extrapulmonary organs [2, 4–6]. Thus, filter media that can effectively capture these harmful fine particles are greatly desired. Fibrous membranes are attractive for particle filtration because they are cost-effective and energy-saving [7]. However, conventional fibers, including glass fibers, melt-blown fibers, and spunbonded fibers, which have been widely used in different air filtration applications, possess a relatively low filtration efficiency with respect to fine particles due to the materials' microsized fiber diameter and large pore size [8, 9]. It is well known that filtration efficiency is greatly enhanced as the fiber diameter decreases [10]. Nanofibers with fiber diameters on the nanoscale are highly capable of capturing ultrafine particles due to their remarkable specific surface area [11]. Electrospinning is an efficient and versatile technique for preparing uniform nanofibers in a continuous process [12–14]. Electrospun nanofibrous membranes exhibit fascinating features, including large specific surface area, high porosity, small pore size, and good interconnected pore structure, which is conducive to the capture of fine particles [15–17]. Exploiting these characteristics, many types of electrospun fibrous membranes have been fabricated as air filtration media. The most common of these are the

homogeneous and single-structured nanofibers, including ultrafine Nylon 6 fibers, polyethylene oxide nanofibers, and alumina nanofibers, which have a circular cross section and a relatively smooth surface [18–20]. These nanofibrous membranes possess high filtration efficiency for fine particles, but they typically have an excessive pressure drop.

It is well known that the collection of fine particles is primarily based on the following mechanisms: Brown diffusion, interception, and inertial impaction [1, 21, 22]. The fiber diameter and morphology of nanofibers, especially the microstructure of its surface, significantly affect the mechanism between the fiber and particles and the penetration of airflow through the fibrous media. Thus, hierarchical structured nanofibers with a high surface roughness have attracted considerable attention to endow the resultant filter media with a high filtration efficiency and a relatively low pressure drop [16, 23–26]. However, few efforts have been focused on the development of an environmentally friendly poly(lactic acid) (PLA) fibrous filter medium with high surface roughness.

In addition to particulate matter, bacteria can also affect human health. Thus, it is very important for the fibrous filter medium to possess antimicrobial properties, especially when they are used as respiratory protection and for indoor air purification [5]. Titanium dioxide (TiO_2) is one of the most popular antibacterial materials, which has been widely used in many fields due to its strong photooxidation activity, long-term chemical and physical stability, and cost-effective preparation [27–29]. Previous studies show that the antibacterial activity of TiO_2 can be significantly enhanced when the TiO_2 particle is on the nanoscale because of its large specific surface area [27, 29]. Thus, considerable efforts have been devoted to the preparation of fiber loaded with TiO_2 nanoparticles to endow the resultant fibrous membrane with antibacterial activity [28, 30, 31]. However, the distribution of TiO_2 NPs on nanofibers dramatically affects the antibacterial performance of the relevant fibrous membrane [28]. It would be very interesting to fabricate a hierarchical nanofiber with TiO_2 nanoparticles uniformly distributed on its surface, which endows the relevant fibrous membrane with not only an excellent filtration performance but also a good antibacterial activity.

In this study, we report the development of a hybrid PLA/TiO_2 fibrous membrane with hierarchical structures, including nanopores, nanometer-scale protrusions, and high surface roughness, which can effectively remove particles and bacteria in one step. The surface microstructure and the distribution of TiO_2 nanoparticles on the fibers were controllable by regulating the concentration of TiO_2 in the PLA solutions, as well as the relative humidity. In addition, the combination of TiO_2 nanoparticles could greatly enhance surface roughness without sacrificing the nanopores on the fiber surface, which significantly improves particle capture efficiency and facilitates the penetration of airflow. More interestingly, the introduction of the TiO_2 nanoparticle and its uniform distribution on the surface of a fiber also endows the relevant fibrous membrane with a good antibacterial performance.

2. Materials and Methods

2.1. Materials. Poly(lactic acid) (PLA $W_m = 1.0 \times 10^5$) was obtained from Zhejiang Hai Zheng Biological Materials Co., Ltd., Zhejiang, China. N,N-Dimethylacetamide (DMAC) was purchased from Sigma-Aldrich, Inc., New Jersey, USA. Dichloromethane (DCM) was purchased from the National Medicine Group Chemical Reagents Co., Ltd., China. TiO_2 NPs (with an average diameter of 21 nm) were supplied by Shanghai Aladdin Chemical Co., China. All of the chemicals were of analytical grade and were used without further purification.

2.2. Preparation of the Polymer Solutions. PLA solutions at concentrations of 7 wt% were prepared by dissolving PLA polymer in a mixture of DCM/DMAC (10/1, w/w) with stirring for 24 h. Additionally, the TiO_2 NPs with an average diameter of 21 nm were added to the mixture of DCM/DMAC (10/1, w/w) with ultrasonic treatment for 90 min and then dissolved PLA polymer in the as-prepared mixture (DCM/DMAC/TiO_2) with stirring for 24 h. The 7 wt% of PLA solutions containing 0.5, 1, 1.5, 1.75, and 2 wt% of TiO_2 NPs was prepared. Furthermore, the PLA/TiO_2 solutions were exposed to ultrasonic treatment for 60 min before electrospinning.

2.3. Electrospinning. The prepared PLA/TiO_2 solution was loaded into a glass syringe and ejected at a controllable feed rate (1 mL/h) through a metal needle with an inner diameter of 850 μm operated by a syringe pump (KDS-100, KD Scientific Co., America). A high voltage (23 kV) was applied to the needle tip through a high-voltage supply (DW-P503-1ACDF, Tianjin Dongwen High Voltage Co., China). The hybrid PLA/TiO_2 fibers were deposited on a grounded metallic rotating roller at 5.5 m/min, which was positioned 12 cm from the tip of the needle.

2.4. Characterization. The viscosity and conductivity of the PLA and PLA/TiO_2 solutions were measured with a viscometer (NDJ-5S, Shanghai Nirun Intelligent Technology Co., Ltd., China) and a conductivity meter (DDS-307A, Shanghai Precision Scientific Instrument Co., Ltd., China), respectively.

2.4.1. Fiber Morphology and Elemental Detection. The morphologies of the electrospun fibers were examined using a field emission scanning electron microscope (FE-SEM) (S-4800, Hitachi Ltd., Japan) and a transmission electron microscope (TEM) (Tecnai G2 F20S-Twin, 120 kV, USA). Energy-dispersive X-ray (EDX) analysis combined with SEM was used to detect the element and the relative surface distribution of TiO_2 nanoparticles on the electrospun fibrous membranes and the randomly selected areas, revealing that the EDX spectra of all of the samples were the same. In addition, the chemical stability of the PLA/TiO_2 fibrous membranes was also investigated using EDX analysis.

2.4.2. Specific Surface Area and Pore Properties. The Brunauer-Emmett-Teller (BET) surface area, pore width, and pore width distribution of the fibrous membranes were measured at 77 K using a nitrogen adsorption-desorption Micromeritics ASAP-2020 analyzer (Micromeritics Co., USA).

2.4.3. Through-Pore Properties. The through-pore size and through-pore size distribution of the fibrous material were measured using a manually operated through-pore size analyzer (Porometer 3G, Quantachrome Ltd., USA).

2.4.4. Testing of Air Filtration Performance. The aerosol filtration efficiency and airflow resistance were measured with a TSI Corp. model 8130 automated filtration testing unit. NaCl aerosol particles with a 260 nm mass median diameter and a 75 nm count median diameter were prepared by an aerosol particle generator. The neutralized NaCl aerosol particles were fed into a filter holder and traveled down through the filter with an effective area of 100 cm^2. Every NaCl aerosol test was conducted at room temperature with a continuous face velocity of 5.3 and 14.1 cm/s.

2.4.5. Photocatalytic Activity Test. The photocatalytic activities of the PLA/TiO_2 fibrous membranes were evaluated by the degradation of methyl orange (MO). The light source was a 300 W self-rectified high pressure Hg lamp. The reaction was maintained at room temperature and the degradation of MO was conducted to guarantee the accuracy of the photocatalytic results. In a typical experiment, aqueous suspensions of MO (50 mL, 2.0×10^{-5} mol/L) and 0.1 g of the as-prepared membranes were placed in the beaker, and the solution was slightly stirred in the dark for 60 min to ensure the establishment of an adsorption-desorption equilibrium. The solution was kept under constant air-equilibrated conditions. Then, at the intervals of given irradiation time, samples of the reaction solution were taken out and analyzed. The decrease in the concentrations of MO was determined by measuring the UV-vis absorbance of the reaction solution.

2.4.6. Antibacterial Efficiency Test. The antibacterial activity of the hybrid PLA/TiO_2 fibrous membranes against *Staphylococcus aureus* was evaluated using the viable cell-counting method as described below according to GB/T 20944.3-2008. Here, the *S. aureus* was first activated with fresh nutrient agar medium and then incubated overnight (18–24 h) at 37°C. Subsequently, the typical colonies were placed in 20 mL of nutrient broth and were incubated at 37°C with gentle shaking (130 rpm) for 18–20 h. The bacterial solution was then diluted to a concentration of approximately 4×10^5 CFU/mL. Typically, the sterilized PLA/TiO_2 fibrous membranes with a weight of 0.75 g were exposed to an *S. aureus* bacterial solution for 24 h at 24°C under visible light. Then, the bacterial solutions were inoculated onto Petri dishes with nutrient agar after tenfold dilutions at 37°C for 24 h. The average number of the surviving bacteria was determined by counting the colonies on the three incubated agar plates for each sample. The antibacterial activity was evaluated based on

$$\text{Antibacterial activity} = \frac{N_{\text{contral}} - N_{\text{sample}}}{N_{\text{contral}}}, \quad (1)$$

where N_{contral} and N_{sample} are the quantities of the visual bacterial colonies of the standard cotton fabric and the tested PLA/TiO_2 composite fibrous membrane, respectively.

3. Results and Discussion

3.1. The Modified Microstructures of the PLA/TiO_2 Fiber and Membrane by Varying the TiO_2 NPs Concentration in the Spinning Solution

3.1.1. Morphologies of Hybrid PLA/TiO_2 Fibers. Figure 1 shows the SEM images of pure PLA fibers and hybrid PLA/TiO_2 fibers obtained by varying the TiO_2 concentration while the other parameters were kept constant (with a feed rate of 1 mL/h and an applied high voltage of 23 kV at a relative humidity of 45%). It was clearly observed that all of the fibers showed densely packed nanopores on their surface, which was due to the phase separation and water droplets or "breath figures" induced by fast solvent evaporation and vapor penetration and condensation [32–34]. By increasing the TiO_2 contents, the surface structure of the hybrid PLA/TiO_2 fibers was remarkably changed by creating nanometer-scale rough structures with additional TiO_2 nanoparticles (TiO_2 NPs) attached onto the surface of fibers without sacrificing the nanopores and the fiber diameters of PLA/TiO_2-0.5, PLA/TiO_2-1, PLA/TiO_2-1.5, PLA/TiO_2-1.75, and PLA/TiO_2-2 slightly increased from 1.29 μm to 1.40 μm with a gradually increasing diameter deviation, which could be ascribed to the weakened conductivity and enhanced viscosity of the composite solutions (Table 1). Furthermore, the TEM images of the corresponding PLA/TiO_2 fibers are displayed in Figure 2. It can be observed that when the TiO_2 concentration was no more than 1.75 wt%, the TiO_2 NPs were relatively evenly distributed on the surface of the fibers, while, as the TiO_2 concentration reached 2 wt%, micron-sized agglomerates formed on the fiber surface, which was related to the agglomeration of TiO_2 NPs (excess TiO_2 NPs in the PLA solution easily aggregated in masses due to their large specific surface area) and the interaction between TiO_2 NPs and the PLA fibers.

SEM-EDX analysis was used to investigate the chemical composition and relative abundance of TiO_2 NPs on the surface of hybrid PLA/TiO_2 fibrous membranes. The elemental composition of the relevant membrane was determined by the EDX spectrum of the randomly selected area (Figure 3). The table insets in the figures list the atomic ratio and weight ratio of the detected elements of the relevant fibrous membranes. The major elements observed were carbon (C), oxygen (O), and titanium (Ti). No Ti peak appeared in the spectrum of the pure PLA fibrous membrane (Figure 2(a)), while the Ti content in spectrum for PLA/TiO_2 fibrous membranes increased as the TiO_2 NP concentration increased (Figures 3(b), 3(c), 3(d), 3(e), and 3(f)), which further confirmed that the TiO_2 NPs were successfully loaded

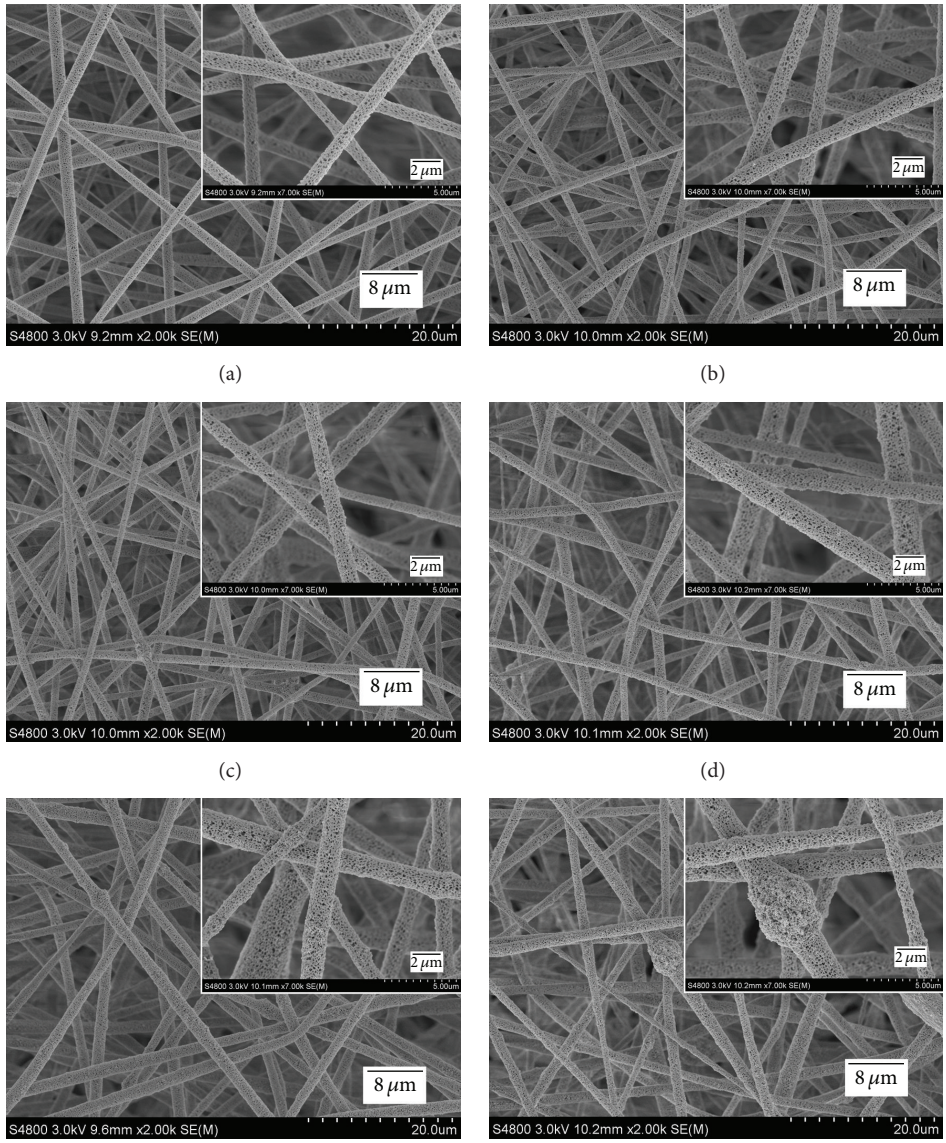

Figure 1: SEM images of (a) PLA, (b) PLA/TiO_2-0.5, (c) PLA/TiO_2-1, (d) PLA/TiO_2-1.5, (e) PLA/TiO_2-1.75, and (f) PLA/TiO_2-2. The insets are the corresponding highly magnified images of each sample.

Table 1: Compositions and properties of different electrospinning solutions and the corresponding fibers.

Sample	Concentration of PLA (wt%)	Concentration of TiO_2 NPs (wt%)	Viscosity (mPa·s)	Conductivity (μs/cm)	Fiber diameter (μm)
PLA	7	0	135	2.65	1.29 ± 0.15
PLA/TiO_2-0.5	7	0.5	144	1.21	1.31 ± 0.17
PLA/TiO_2-1	7	1	158	0.86	1.33 ± 0.20
PLA/TiO_2-1.5	7	1.5	178	0.71	1.34 ± 0.22
PLA/TiO_2-1.75	7	1.75	202	0.62	1.36 ± 0.24
PLA/TiO_2-2	7	2	236	0.54	1.40 ± 0.30

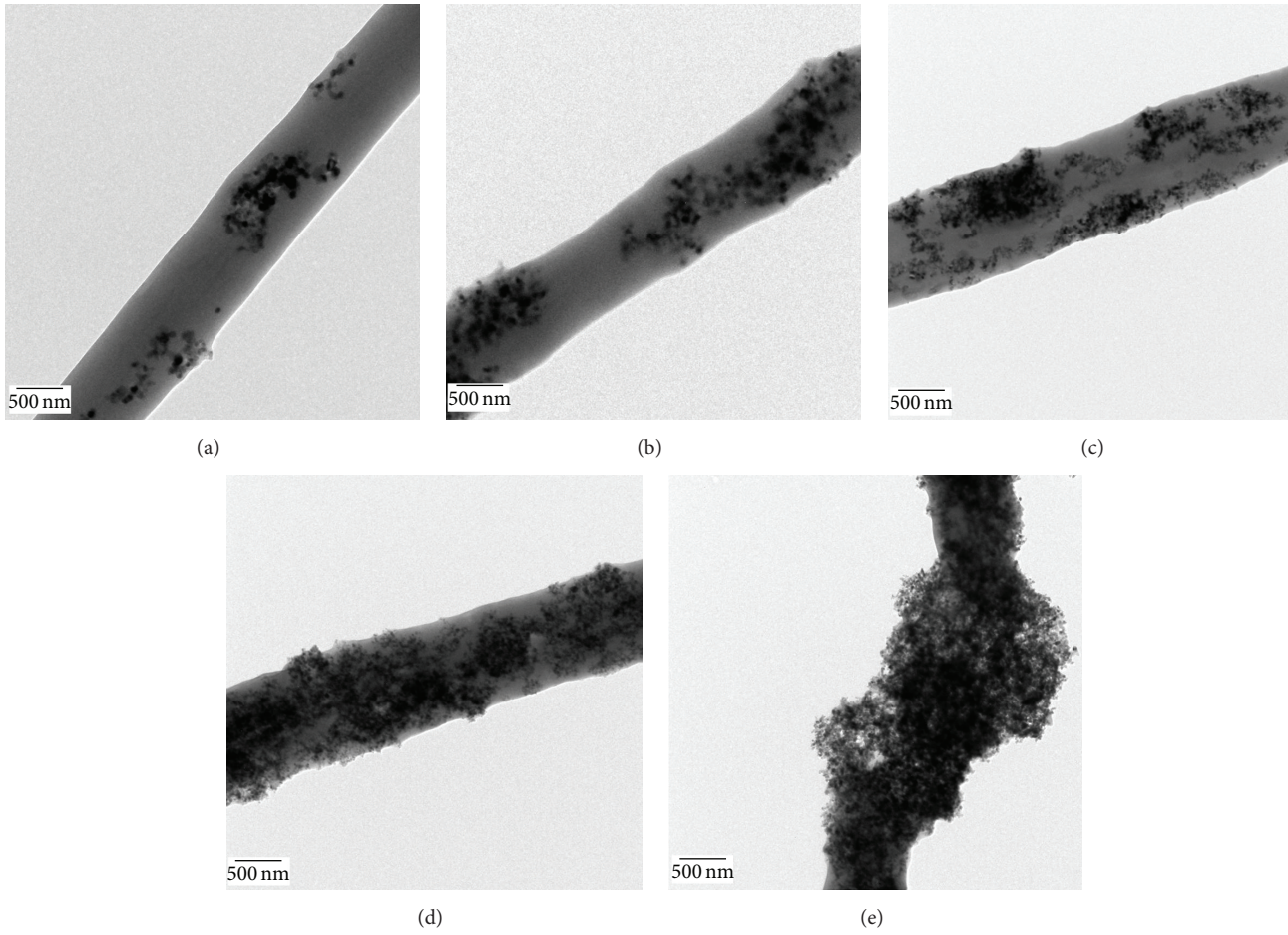

Figure 2: TEM images of (a) PLA/TiO_2-0.5, (b) PLA/TiO_2-1, (c) PLA/TiO_2-1.5, (d) PLA/TiO_2-1.75, and (e) PLA/TiO_2-2.

onto the PLA fibers. Higher elemental signal counts of Ti suggested a higher amount of TiO_2 NP additives on the surface of the relevant fibrous membrane, which agreed well with the results shown in Figures 1 and 2. The atomic ratio and weight ratio of Ti increased with increasing TiO_2 contents, as shown in the tables shown as an inset in the corresponding Figures 3(b), 3(c), 3(d), 3(e), and 3(f).

3.1.2. Porous Structure and BET Surface Area of Hybrid PLA/TiO_2 Fibrous Membrane. It is well known that the morphologies of the fibers significantly affected the specific surface area and the nanoporous structure of the resultant fibrous membrane [26, 35, 36]. In addition to the nanopore formed on the surface of the fibers, the protuberant structures induced by the introduction of TiO_2 NPs may also enhance the surface roughness and specific surface area, which may dramatically increase the friction coefficient and the effective contact area between target particles and fibers when the relevant fibrous membrane was used as an air filter medium. Thus, the nitrogen adsorption-desorption isotherms and pore size distribution curves of the PLA fibrous membrane loaded with various contents of TiO_2 NPs were obtained to investigate their specific surface area and nanopore structure, as shown in Figure 4.

All of the samples have isotherms of type II with a distinct hysteresis loop, according to the International Union and Applied Chemistry (IUPAC) classification, which indicated the presence of mesopores (2–50 nm pore width) and macropores (>50 nm pore width) within the samples [35, 37, 38]. The BET surface area and Barrett-Joyner-Halenda (BJH) adsorption cumulative nanopore volume of the as-prepared samples are shown in the table inset of Figure 4(a). The BET surface area and BJH adsorption cumulative nanopore volume experienced a steady growth with increasing TiO_2 contents (the concentration of TiO_2 NPs was no more than 1.75 wt%), which indicated the key role of TiO_2 NPs in improving the specific surface area; this was consistent with the increased quantity of adsorbed N_2. It is noteworthy that the BET surface area and BJH adsorption cumulative nanopore volume of the PLA/TiO_2-2 fibrous membrane were slightly lower than those of the PLA/TiO_2-1.75 fibrous membrane. This phenomenon could be attributed to the formation of large agglomerates on the surface of PLA/TiO_2-2 fibers. The nanopore size distributions were also obtained by applying the BJH method to the nitrogen adsorption

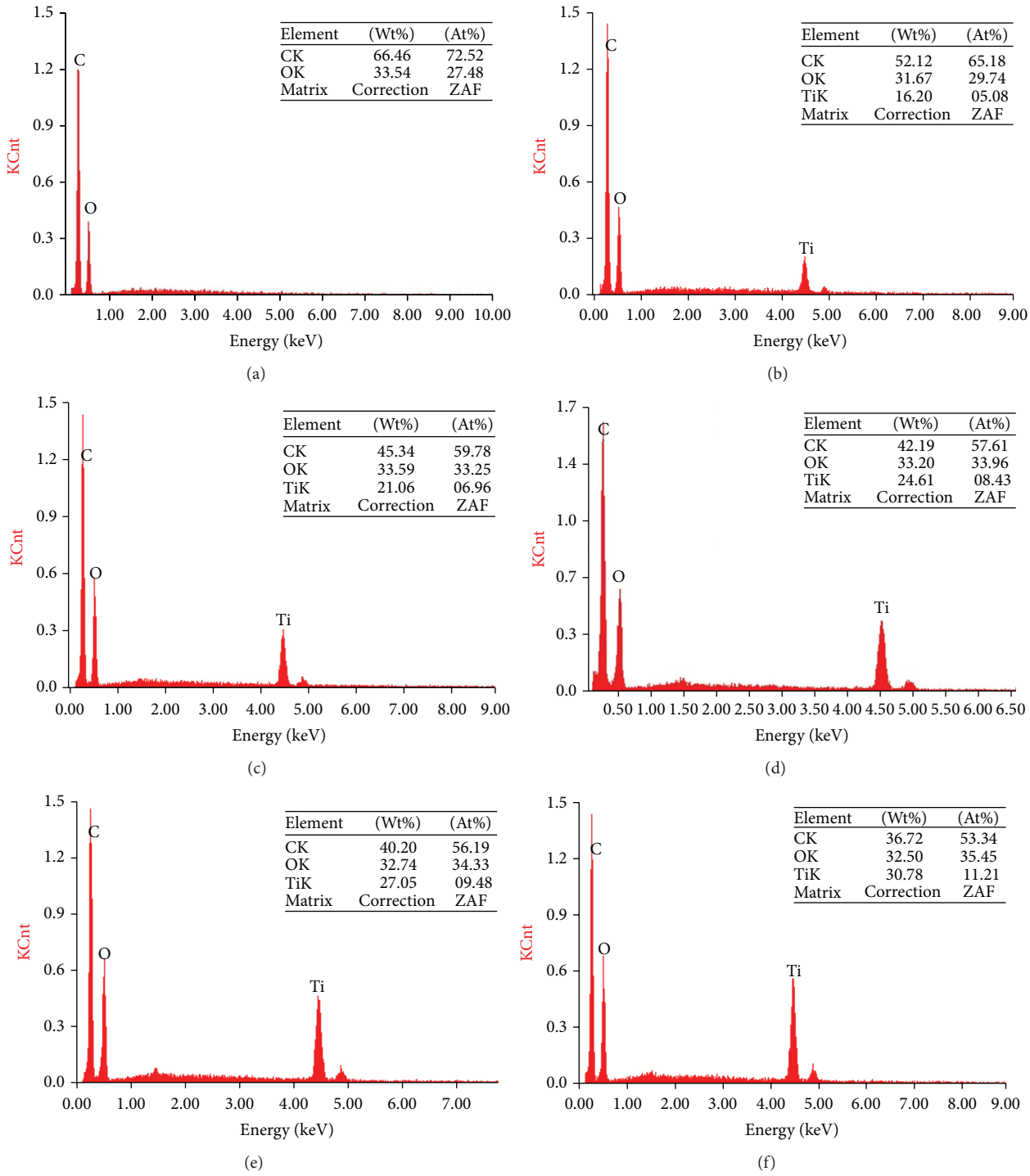

FIGURE 3: SEM-EDX spectra of (a) PLA, (b) PLA/TiO_2-0.5, (c) PLA/TiO_2-1, (d) PLA/TiO_2-1.5, (e) PLA/TiO_2-1.75, and (f) PLA/TiO_2-2 fibrous membranes. The inset tables are the corresponding atomic ratio and weight ratio of the detected elements.

isotherms, as shown in Figure 4(b). It was clearly seen that the pores were mainly distributed in the range of 10 to 120 nm. Thus, the pores formed in the samples were highly dependent on the nanopores and the protuberances on the surface of the fibers. The pore volumes of the pure PLA fibrous membrane in the mesopore range were larger than those in the macropore range, which may suggest that the pores in the sample were mainly caused by the nanopores on the fiber surface. The pore volumes of the hybrid PLA/TiO_2 fibrous membranes in the mesopore range were lower than those in the macropore range. Furthermore, the pore volumes in the macropore range increased with the increase of TiO_2 contents attached onto the PLA fibers when the concentration of TiO_2 NPs was less than 2 wt%, which may be ascribed to the enhanced

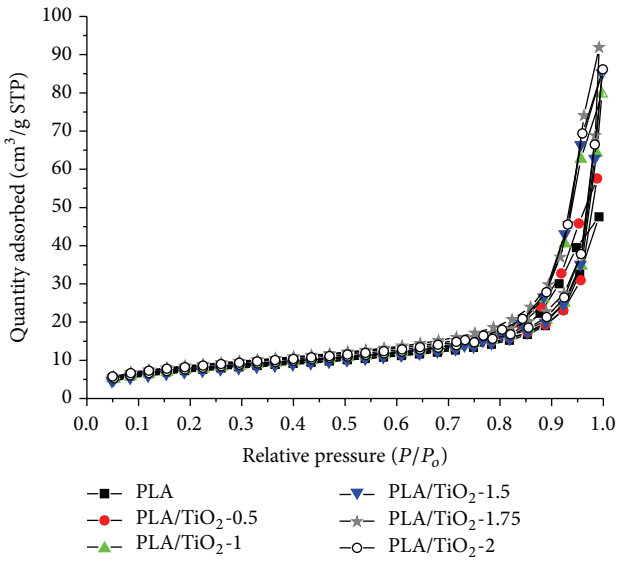

(a)

Sample	BET surface area (m^2/g)	BJH adsorption cumulative volume of pores (m^3/g)
PLA	21.86	0.073
PLA/TiO_2-0.5	23.75	0.086
PLA/TiO_2-1	26.11	0.111
PLA/TiO_2-1.5	27.89	0.125
PLA/TiO_2-1.75	30.54	0.139
PLA/TiO_2-2	28.84	0.130

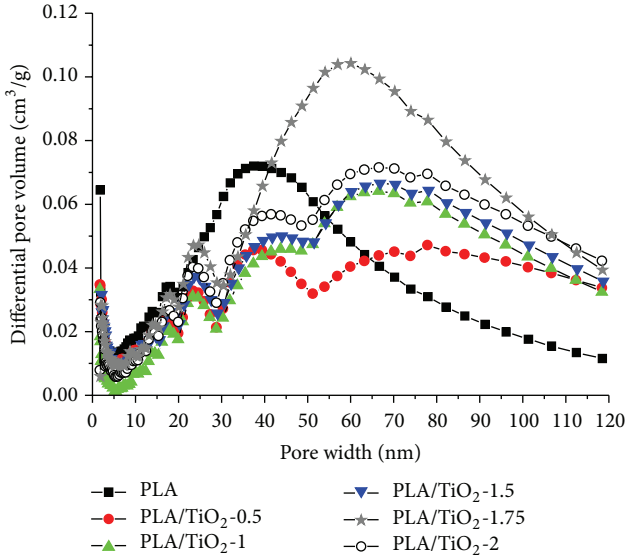

(b)

Figure 4: (a) Nitrogen adsorption-desorption isotherms of hybrid PLA/TiO_2 fibrous membranes loaded with various TiO_2 NPs contents. (b) Pore size distribution curves of the corresponding hybrid PLA/TiO_2 fibrous membranes.

roughness, the gradually increased protuberances, and the larger nanopores on the surface of the fibers induced by the incorporation of TiO_2 NPs. The micron-sized agglomerates formed on the surface of PLA/TiO_2-2 fibers may lead to the fact that the pore volumes of the relevant fibrous membrane in the mesopore and macropore range were lower than those of the PLA/TiO_2-1.75 fibrous membrane.

3.2. The Modified Microstructures of the PLA/TiO_2 Fiber and Membrane by Varying the Ambient Relative Humidity (RH)

3.2.1. The Morphologies and Distributions of TiO_2 NPs on PLA/TiO_2 Fibers Formed under Different RHs. Figure 5 displays the SEM images of hybrid PLA/TiO_2 fibers loaded with 1.75 wt% TiO_2 NPs prepared by varying the relative humidity (RH), 15%, 30%, 45%, and 60%, with the other parameters maintained constant (Table 2). It could be found that the morphologies of the fibers were significantly changed with the variation of the RH. As shown in Figure 5(a), the fibers formed under a RH of 15% possessed few shallow nanopores and more protuberances on its surface with a large diameter deviation (Table 2). The nanopores distributed on the surface of the fibers increased with the increase of the RH (Figures 5(b) and 5(c)), which could be because a high RH allows much more vapor in the air to form more water droplets on the surface of the jet and is conducive to the penetration of much more vapor into the fluid jet [34, 39]. The average fiber diameters sharply increased from 0.76 μm to 1.36 μm

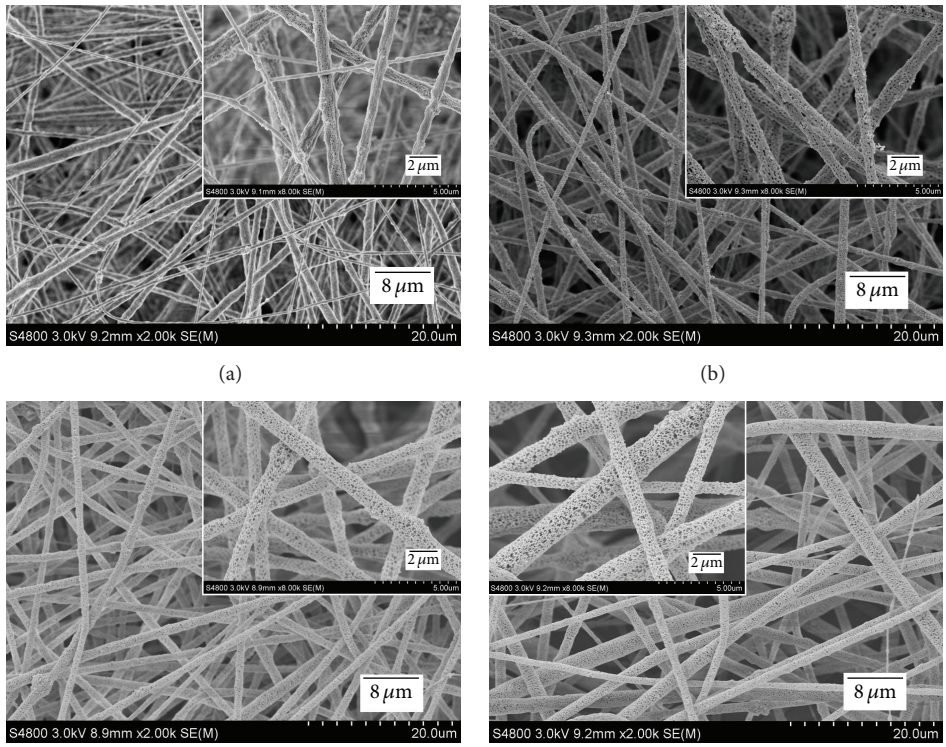

Figure 5: SEM images of the PLA/TiO_2 fibrous membranes loaded with 1.75 wt% TiO_2 NPs fabricated under various relative humidities: (a) 15%, (b) 30%, (c) 45%, and (d) 60%. The insets are the corresponding highly magnified images of each sample.

Table 2: Electrospun parameters and properties of the corresponding fibers.

Sample	Relative humidity (%)	High voltage (kV)	Feed ratio (mL/h)	Fiber diameter (nm)
PLA/TiO_2-15%	15	23	1	0.76 ± 0.34
PLA/TiO_2-30%	30	23	1	0.98 ± 0.26
PLA/TiO_2-45%	45	23	1	1.36 ± 0.24
PLA/TiO_2-60%	60	23	1	1.43 ± 0.30

with the fiber becoming more uniform as the RH gradually reached 45%. This phenomenon may be because under a too low RH condition, the electrostatic repulsion applied to the fluid jet was relatively high because the applied high voltage was the same, and the Taylor cone and capillary were unstable, which led to the formation of thinner fibers with a large diameter deviation. When the RH reached 60%, an excessively high RH may weaken the electrostatic repulsion and oppose the balance between the viscoelastic force, surface tension, and electrostatic repulsion, resulting in thicker fibers with a relative large diameter deviation. To further study the effect of RH on the distribution of TiO_2 NPs on the surface of the PLA fiber, TEM analyses were performed on the hybrid PLA/TiO_2 fibers loaded with 1.75 wt% TiO_2 NPs formed under different RHs, as shown in Figure 6. This figure clearly shows that more protrusions formed on the surface of the fibers under the RH of 15% and 30%, and the protrusions attached onto the surface of the fibers decreased as the RH gradually increased to 60%, which may be because the increase in the fiber diameter (Table 2) provided more opportunity for the TiO_2 NPs to distribute inside of the fibers. However, TiO_2 NPs were more uniformly distributed on the surface of the fibers prepared at the relative humidity of 45% and 60%.

To further investigate the relative abundance of TiO_2 NPs on the surface of hybrid PLA/TiO_2 fibrous membranes, SEM-EDX analyses were performed, and the EDX testing data are shown in Figure 7. It can be observed that the content of Ti in the spectrum of the hybrid PLA/TiO_2 fibers was weakened, and the atomic ratio and weight ratio of Ti gradually decreased with the increase of RH, which suggests that the TiO_2 NPs that were distributed on the surface of the hybrid PLA/TiO_2 fibrous membrane decreased. This phenomenon agreed with the results shown in Figures 5 and 6 in which fewer TiO_2 NPs were distributed on the surface of the PLA fibers due to the increase of the fiber diameter by increasing the RH. Thus, it can be concluded that the TiO_2 NPs prefer to distribute on the surface of the PLA/TiO_2 fibrous membrane when the precursor PLA/TiO_2 solution was electrospun under a low RH.

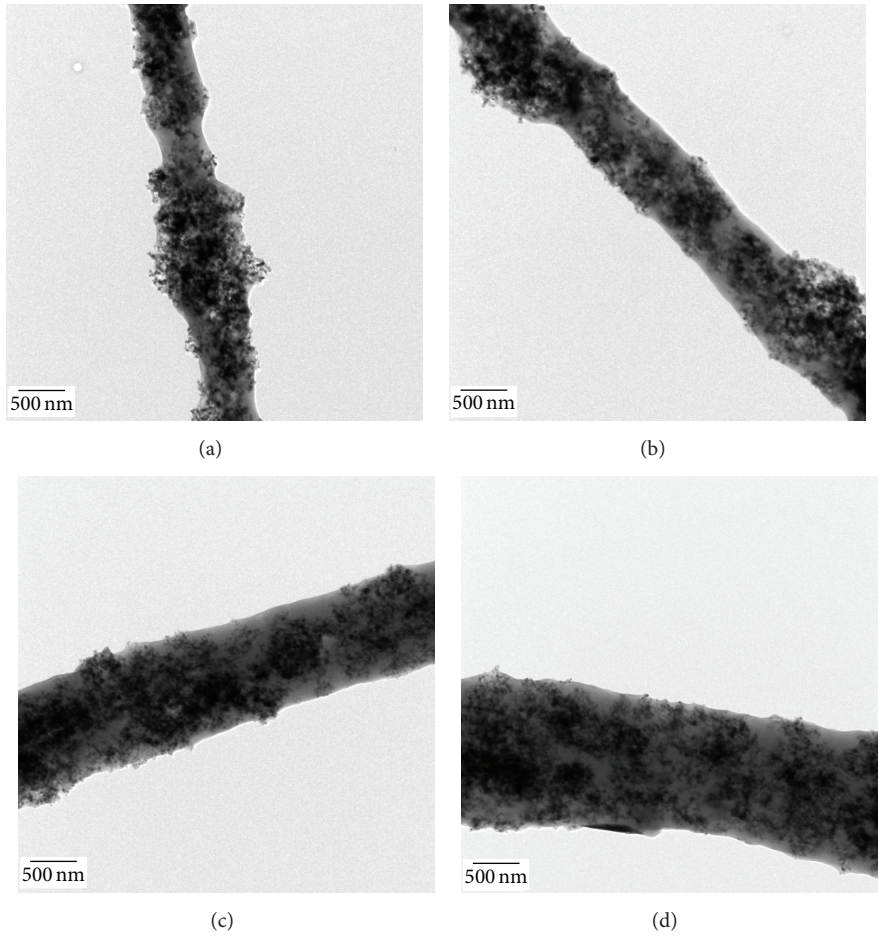

Figure 6: TEM images of the PLA/TiO_2 fibrous membranes loaded with 1.75 wt% TiO_2 NPs fabricated under various relative humidities: (a) 15%, (b) 30%, (c) 45%, and (d) 60%.

3.2.2. Porous Structure and BET Surface Area of a Hybrid PLA/TiO_2 Fibrous Membrane Electrospun under Different RHs. The RH has a dramatic effect on the morphology of hybrid PLA/TiO_2 fibers, as shown in Figure 5, which may result in very different nanoporous structures and BET surface areas of the corresponding fibrous materials. To characterize the pore structure and specific surface area of the hybrid PLA/TiO_2 fibrous membranes, the nitrogen physisorption method was used, and the testing results are shown in Figure 8. As seen, the nitrogen physisorption isotherms of all of the samples show a type II isotherm with a hysteresis loop, indicating the existence of mesopores and macropores within the fibrous membranes. The table inset in Figure 8(a) presents the BET surface area and cumulative nanopore volume calculated by the BJH method, which shows that the specific surface area of the PLA/TiO_2 fibrous membrane formed under a RH of 45% (PLA/TiO_2-45%) is approximately 1.58 times and 1.2 times that of the fibrous membranes prepared under a RH of 15% and 30%, respectively. This phenomenon can be ascribed to the significant increase of nanopores on the surface of the fibers, although the fiber diameter has increased. Furthermore, the cumulative nanopore volume of the hybrid PLA/TiO_2 fibrous membranes increased from 0.078 to 0.139 m^3/g when the relative humidity varied from 15% to 45%. It is worth noting that the specific surface area and cumulative nanopore volume of the hybrid PLA/TiO_2 fibrous membrane formed under a RH of 60% (PLA/TiO_2-60%) were slightly lower than those of PLA/TiO_2-45%, which can be attributed to the decrease of protuberances induced by the TiO_2 NPs on the surface of the fibers and the slight increase in the fiber diameter. Figure 8(b) shows the differential pore volume versus the pore width of the relevant hybrid PLA/TiO_2 fibrous membranes. It can be found that the pores existing within the membranes mainly range from 10 nm to 120 nm. The pore volume of the pore width larger than 10 nm tended to increase rapidly as the RH increased from 15% to 45%, and the pore volume of the pore width in macropore range decreased when the RH increased from 45% to 60%. This phenomenon is in good agreement with the variation trend of the cumulative nanopore volume of the relevant PLA/TiO_2 fibrous membrane.

3.3. Air Filtration Performances of Hybrid PLA/TiO_2 Fibrous Membranes with Different Morphologies. It is well known that electrospun fibers have been widely used in many fields,

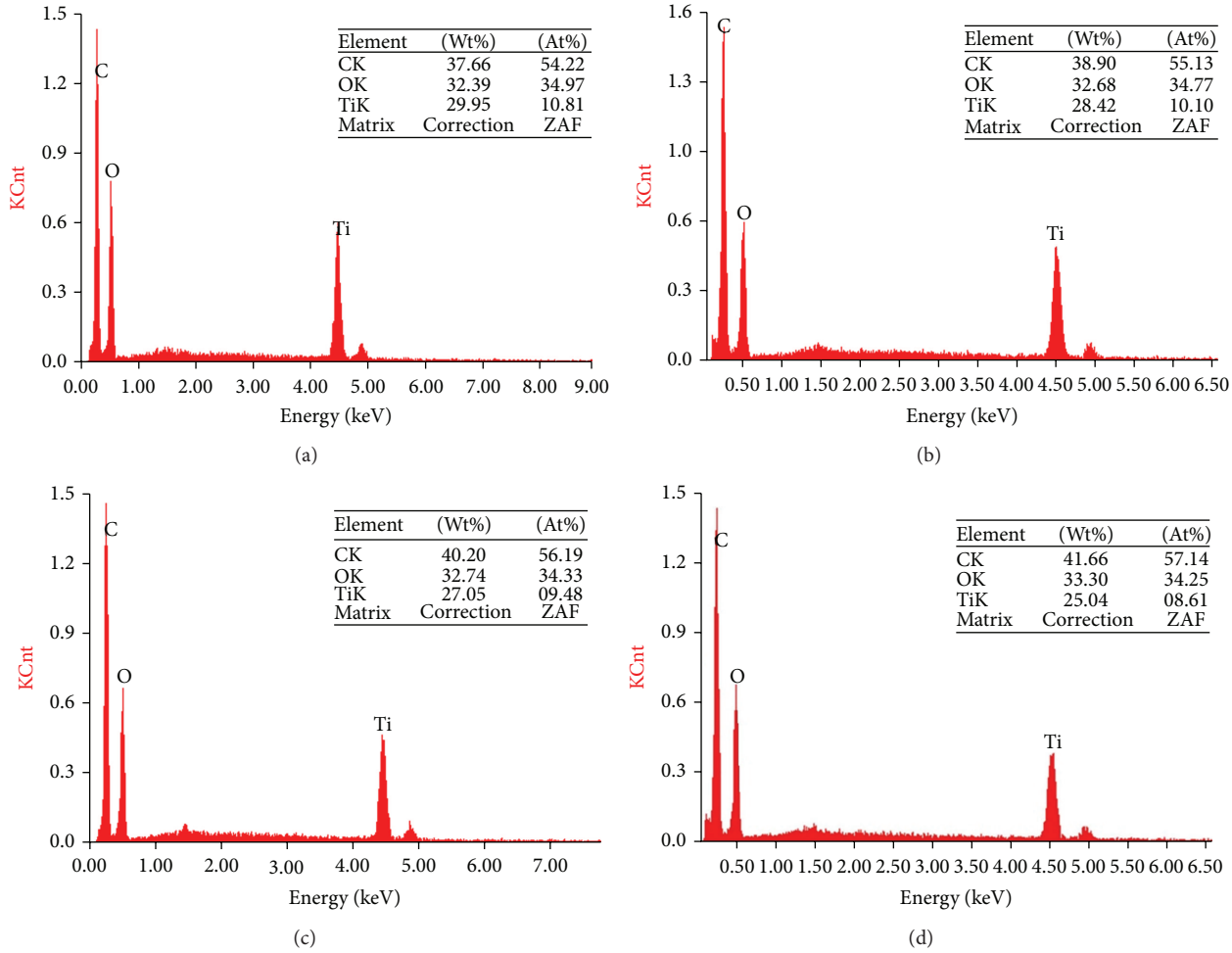

FIGURE 7: SEM-EDX spectra of the PLA/TiO_2 fibrous membranes loaded with 1.75 wt% TiO_2 NPs fabricated under various relative humidities: (a) 15%, (b) 30%, (c) 45%, and (d) 60%. The inset tables are the corresponding atomic ratio and weight ratio of the detected elements.

especially in air filtration. The hybrid PLA/TiO_2 fibers possess high surface roughness (many nanopores and nanometer-scale protrusions distributed on the surface of the fibers), significantly large specific surface area, and small fiber diameter, which would provide the relevant fibrous membrane with a higher probability of capturing the target particles, finally enhancing the filtration performance. Thus, the hybrid PLA/TiO_2 fibrous membranes, FM1 (containing 0 wt% TiO_2 prepared at the relative humidity of 45%), FM2 (containing 1 wt% TiO_2 prepared at the relative humidity of 45%), FM3 (containing 1.75 wt% TiO_2 prepared at the relative humidity of 45%), FM4 (containing 1.75 wt% TiO_2 prepared at the relative humidity of 15%), and FM5 (containing 1.75 wt% TiO_2 prepared at the relative humidity of 60%), with different morphologies and possessing similar basis weights (Table 3) were selected to study their air filtration performance.

3.3.1. Through-Pore Characteristics. The thorough-pore size and through-pore size distribution are very important parameters to determine the air filtration performance of the fibrous filter. Thus, these parameters of the hybrid PLA/TiO_2 fibrous membranes were measured using a manually operated through-pore size analyzer, as shown in Figure 9. The mean flow through-pore sizes of these samples were 5.14, 5.31, 5.46, 4.85, and 5.70 μm, respectively (Table 3). The results clearly demonstrated that the pore sizes decreased as the TiO_2 contents increased, which could be due to the increase in the fiber diameter and the increased protrusions attached on the fiber surface, resulting in relatively large voids between fibers. Furthermore, the pore size distribution of the relevant membranes became gradually broader. In addition, the pore size experienced a significant increase and showed a broad pore size distribution with the increase of RH when FM3 was compared with FM4 and FM5. This phenomenon could be ascribed to the increase in the fiber diameter.

3.3.2. Air Filtration Performances. To thoroughly comprehend the inherent correlation between the filtration performance and morphology, including the nanopores and protrusions on the fiber surface and the fiber diameter, of the hybrid PLA/TiO_2 fibrous membranes, the filtration efficiency and pressure drop of the selected fibrous membranes (FM1,

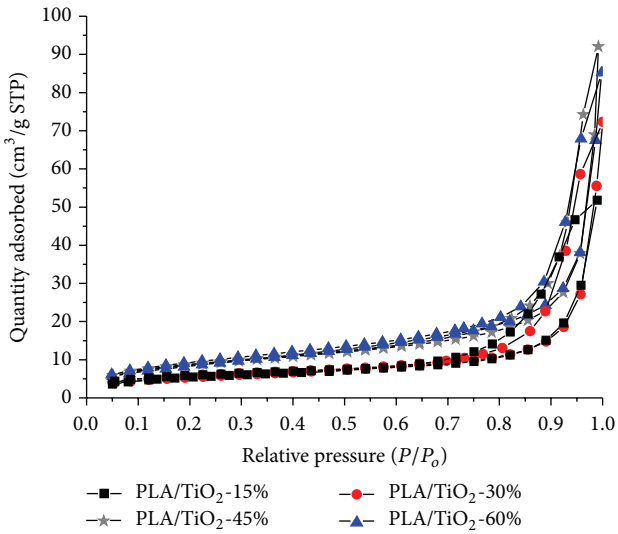

(a)

Sample	BET surface area (m^2/g)	BJH adsorption cumulative volume of pores (m^3/g)
PLA/TiO_2-15%	19.27	0.078
PLA/TiO_2-30%	25.36	0.097
PLA/TiO_2-45%	30.54	0.139
PLA/TiO_2-60%	28.06	0.129

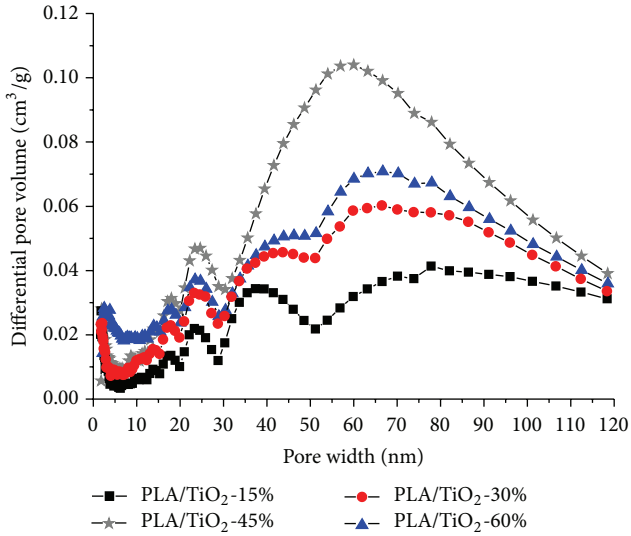

(b)

Figure 8: (a) Nitrogen adsorption-desorption isotherms of hybrid PLA/TiO_2 fibrous membranes loaded with 1.75 wt% TiO_2 NPs formed at various relative humidities: 15%, 30%, 45%, and 60%. (b) Pore size distribution curves of the corresponding hybrid PLA/TiO_2 fibrous membranes.

Table 3: Characterization and formed parameters of the PLA/TiO_2 fibrous membranes with different morphologies.

Sample	Concentration of TiO_2 NPs (wt%)	Humidity (%)	Basis weights (g/m^2)	Mean flow through-pore size (μm)
FM1	0	45	6.30	5.14
FM2	1	45	6.33	5.31
FM3	1.75	45	6.28	5.46
FM4	1.75	15	6.24	4.85
FM5	1.75	60	6.27	5.70

FM2, FM3, FM4, and FM5) were evaluated by filtering NaCl aerosol particles of 260 nm in mass median diameter.

The pressure drop and filtration efficiency of the hybrid PLA/TiO_2 fibrous membranes loaded with various contents of TiO_2 NPs (FM1, FM2, and FM3) as a function of a face velocity of 14.1 cm/s and 5.3 cm/s are shown in Figure 10(a). It can be observed that the resultant hybrid PLA/TiO_2 fibrous membranes exhibited increased filtration efficiency and, more significantly, a decreased pressure drop with the increase of the concentration of TiO_2 NPs. These results were due to the increase of the nanometer-scale protrusions and the roughness of the fiber surface, resulting in a high

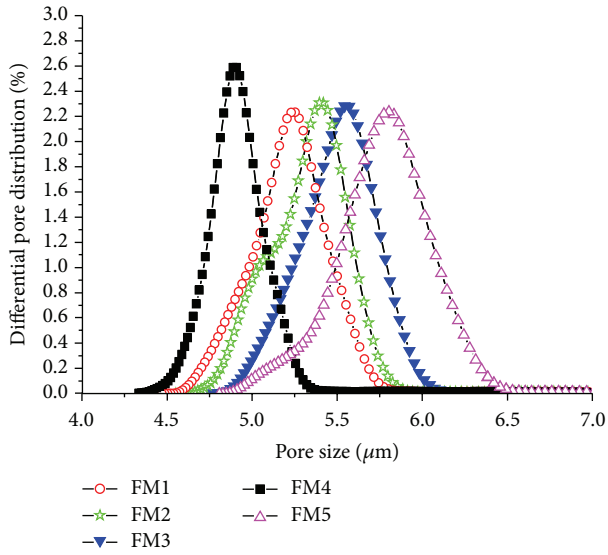

Figure 9: Through-pore size distribution curves of FM1, FM2, FM3, FM4, and FM5.

specific surface area and large friction coefficient, which enhanced the trapping capacity of the fibers on the particles. Furthermore, the relatively large through-pore size induced by the thicker fiber and high cumulative nanopore volume may be conducive to the penetration of airflow through the membranes [7, 25]. This phenomenon contradicts the traditional theory about the trade-off between filtration efficiency and pressure drop in which a high filtration efficiency typically results in a high pressure drop, further indicating the key role of nanopores and protrusions on the fiber surface in improving the filtration performance of the relevant fibrous membrane. According to the previous studies, the quality factor (QF) was typically used as a comprehensive parameter to judge the filtration performance of a filter. QF is defined as $\mathrm{QF} = -\ln(1-\eta)/\Delta p$, where η and Δp are the filtration efficiency and pressure drop across the filter, respectively. Due to the improvement in the filtration efficiency and the decreased pressure drop, the QF of hybrid PLA/TiO_2 fibrous membranes displayed in Figure 10(a) experienced a steady increase with the increase of TiO_2 contents at a face velocity of 14.1 cm/s (from 0.023 to 0.028) and 5.3 cm/s (from 0.066 to 0.078).

Figure 10(b) presents the filtration performance of hybrid PLA/TiO_2 fibrous membranes containing 1.75 wt% TiO_2 formed at various relative humidities (15%, 45%, and 60%). It is shown that the fibrous filter FM4 exhibited the lowest filtration efficiency (99.965%) and the highest pressure drop (375.5 Pa), reasonably resulting in the lowest QF (0.021) of the three membranes at the face velocity of 14.1 cm/s. This result could be because the relatively low specific surface area and the few nanopores on the fiber surface induced by a low RH weakened the fiber's capture efficiency of fine particles, and the small and narrowly distributed through-pore size due to the small fiber diameter may go against the air penetration. This is also the reason that FM4 showed the worst filtration performance at a face velocity of 5.3 cm/s. It is worth noting that the filtration efficiency of FM5 was 99.972% at a face velocity of 14.1 cm/s and 99.994% at a face velocity of 5.3 cm/s. These values were slightly lower than those of FM3 (99.990% and 99.996% at a face velocity of 14.1 and 5.3 cm/s, resp.) at the corresponding face velocity due to a relatively small specific surface area, few protrusions, and large fiber diameter. Furthermore, the pressure drop of FM5 was 313.8 Pa and 119.7 Pa at a face velocity of 14.1 cm/s and 5.3 cm/s, respectively, which were also lower than those of FM3 (326.9 Pa and 128.7 Pa at a face velocity of 14.1 and 5.3 cm/s, resp.) at the corresponding face velocity due to a larger and broadly distributed through-pore size. Interestingly, the QF of FM5 was lower than that of FM3 at a face velocity of 14.1 cm/s, while it was slightly higher than that of FM3 at a face velocity of 5.3 cm/s. This phenomenon indicates that FM5 exhibited a better filtration performance at a low face velocity.

These observations led us to conclude that the nanopores and nanometer-scale protrusions resulting in high structure roughness, large specific surface area, and cumulative nanopore volume of the relevant fibrous membrane on the surface of the fibers enhanced the particle capture efficiency and contributed to the decrease of the pressure drop, which significantly improved the filtration performance. This also provided a new approach to develop and design a fibrous filter possessing a high filtration efficiency and energy-saving ability by controlling the surface structure and fiber diameter of the relevant fibers.

3.4. Photocatalytic Activity. The photocatalytic activities of the as-prepared PLA/TiO_2 fibrous membranes (FM1, FM2, FM3, FM4, and FM5) were investigated by evaluating their photodegradation performance towards methyl orange (MO) at room temperature. Figure 11 shows the time course of the decrease in the concentration of MO under the UV irradiation of 300 W high pressure Hg lamp. It can be seen that the MO solution was stable with negligible degradation (<3%) under the pristine PLA fibrous membrane (FM1) condition. The photocatalytic activity of the hybrid PLA/TiO_2 fibrous membranes (FM2 and FM3) improved significantly with the increase of the TiO_2 NPs content, and the FM3 could degrade the MO up to 97% within 150 min. This phenomenon could be contributed to the increase of anatase TiO_2 NPs on the surface of PLA/TiO_2 fibrous membranes, which could simultaneously degrade MO. In addition, the photocatalytic activities of the PLA/TiO_2 fibrous membranes (FM4, FM3, and FM5) loaded with 1.75 wt% TiO_2 NPs gradually weaken with increasing the relative humidity, and FM4 could degrade the MO completely within 150 min. This phenomenon is in agreement with the previous results in which more TiO_2 NPs were distributed on the surface of PLA/TiO_2 fibrous membrane with an increase of the relative humidity.

3.5. Antibacterial Activity of Hybrid PLA/TiO_2 Fibrous Membranes with Different Morphologies. Next, an investigation into the effect of TiO_2 NPs and their distribution on PLA fibers for antibacterial application was performed. The antibacterial activity of the pure PLA fibrous and PLA/TiO_2

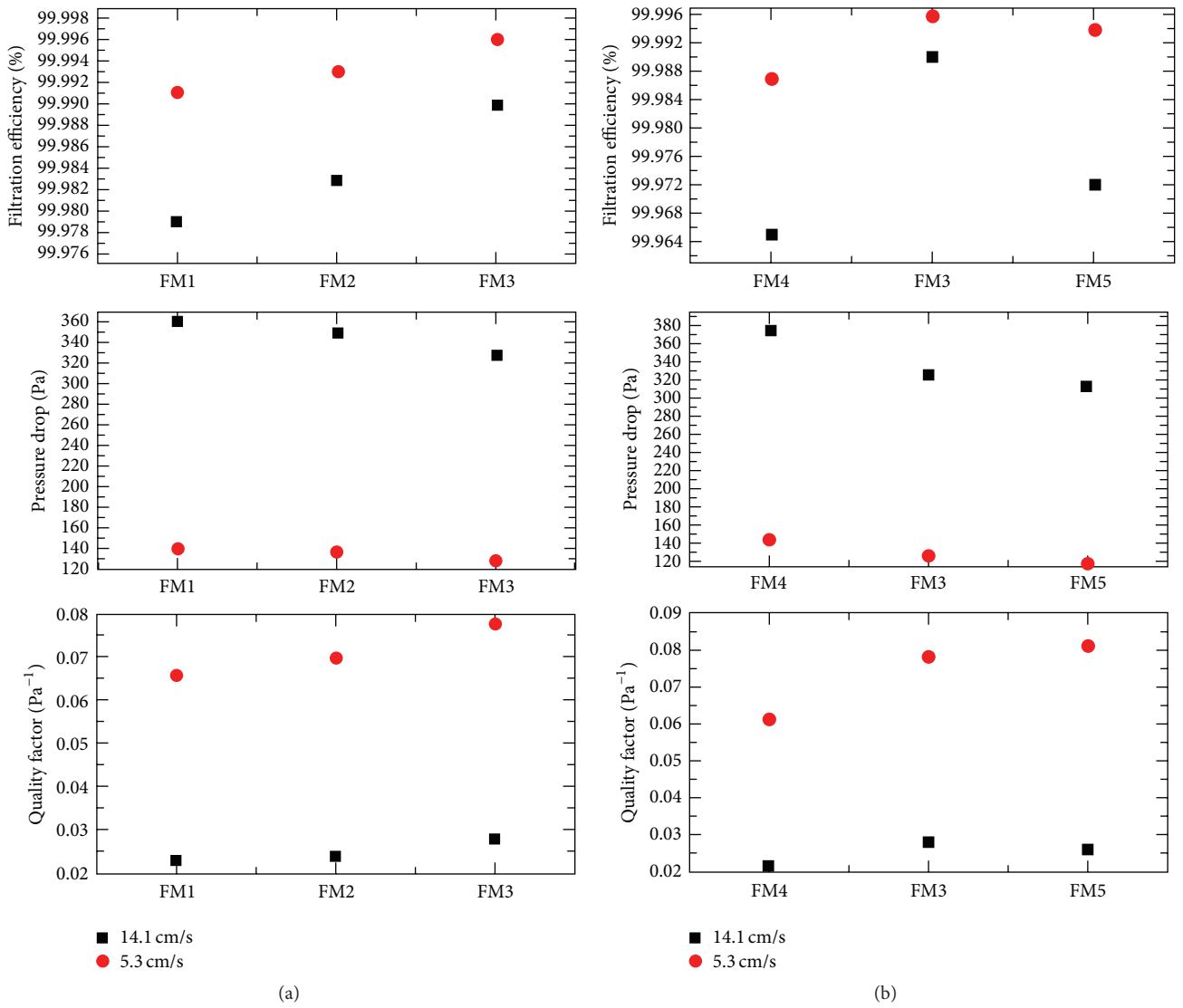

Figure 10: Filtration performance of FM1, FM2, FM3, FM4, and FM5 at various face velocities: (a) filtration efficiency, pressure drop, and quality factor of FM1, FM2, and FM3 at a face velocity of 5.3 cm/s and 14.1 cm/s; (b) filtration efficiency, pressure drop, and quality factor of FM3, FM4, and FM5 at a face velocity of 5.3 cm/s and 14.1 cm/s.

fibrous membranes with different morphologies against *S. aureus* is illustrated in Figure 12. It was observed that the antibacterial activity of PLA fibrous membranes significantly increased by increasing the TiO_2 NPs content. The pure PLA fibrous membrane (FM1) with no TiO_2 NPs showed an antibacterial activity of only 10.1%. The hybrid PLA/TiO_2 fibrous membrane decorated with 1 wt% TiO_2 NPs (FM2) showed approximately 74.8% antibacterial activity. A reduction by approximately 99.5% was observed in bacterial growth for the hybrid PLA/TiO_2 fibrous membrane loaded with 1.75 wt% TiO_2 NPs (FM3). These results may be because more TiO_2 NPs were distributed on the surface of PLA fibers with the increase of TiO_2 NPs content and because the reactive hydroxyl radicals generated by the photocatalysis of TiO_2 NPs under light irradiation cause the peroxidation of the polyunsaturated phospholipid of the bacteria cell membrane, leading to a loss of respiratory activity, which kills the bacteria [27, 29]. It is worth noting that the hybrid PLA/TiO_2 fibrous membrane decorated with 1.75 wt% TiO_2 NPs formed at a relative humidity of 15% (FM4) possesses 99.8% antibacterial activity, which was slightly higher than that of FM3. In addition, the antibacterial activity of FM5 formed at the relative humidity of 60% is 97.4%, which is slightly lower than that of FM3. This phenomenon agrees well with the photocatalytic activity testing results.

3.6. The Chemical Stability of the Hybrid PLA/TiO_2 Fibrous Membrane. To investigate the chemical stability of the hybrid PLA/TiO_2 fibrous membranes (FM1, FM2, FM3, FM4, and FM5), SEM-EDX analyses were also performed, and the EDX testing data of the corresponding membranes after exposure under visible light for 30 days are shown in Figure 13. It can

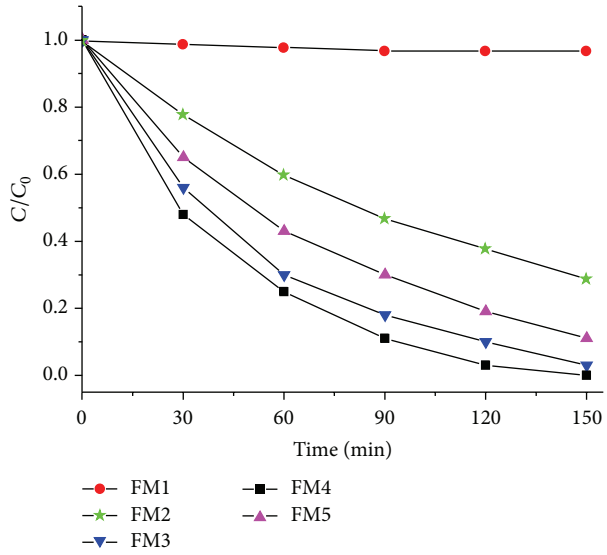

Figure 11: Photocatalytic degradation profiles of MO with various fibrous membranes (FM1, FM2, FM3, FM4, and FM5, resp.).

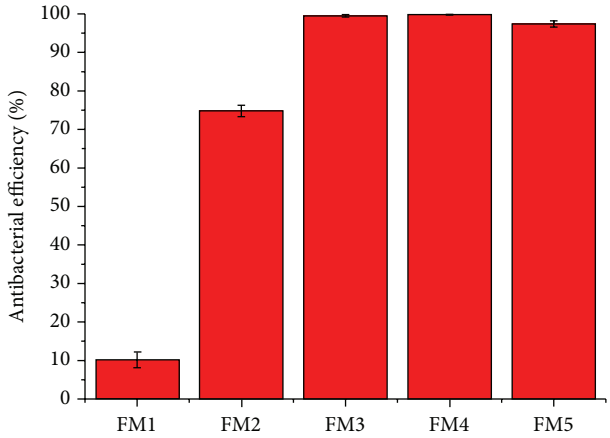

Figure 12: Antibacterial activity of FM1, FM2, FM3, FM4, and FM5 against *S. aureus*. The control consists of cotton fabric placed in a Petri dish under the same treatment conditions. The error bars represent the ± standard error of the mean.

be observed that the contents of C and O in the spectrum of the PLA fibrous membrane were almost the same as those of the previously prepared PLA fibrous membrane shown in Figure 3(a). In addition, the contents of C, O, and Ti of the hybrid PLA/TiO_2 fibrous membranes were very similar to those of the corresponding hybrid PLA/TiO_2 fibrous membranes prepared 30 days before, which suggests that the hybrid PLA/TiO_2 fibrous membranes possess good chemical stability.

4. Conclusions

In summary, a hierarchical structure of PLA/TiO_2 fibers for enhanced air filtration performance with good antibacterial activity was prepared via a one-step electrospinning technique. The microstructure, including the nanopores and nanometer-scale protrusions on the fiber surface, and the distribution of TiO_2 in hybrid PLA/TiO_2 can be regulated by tuning the concentration of TiO_2 NPs in the PLA solution and the relative humidity. Furthermore, the nanopores and nanometer-scale protrusions on the PLA fiber significantly enhanced the surface roughness, the specific surface area, and the cumulative nanopore volume of the relevant fibrous membrane, which greatly improved the particle capture efficiency and facilitated the penetration of airflow. In addition, the introduction of TiO_2 NPs endows the relevant fibrous membrane with antibacterial properties induced by photocatalysis, and additional TiO_2 NPs distributed on the surface of the fibrous membrane indicated a higher photocatalytic activity and antibacterial activity. Furthermore, the PLA/TiO_2 also possessed good chemical stability. The as-prepared PLA/TiO_2 fibrous membrane loaded with 1.75% TiO_2 NPs formed at a relative humidity of 45% exhibited excellent filtration performances with a high filtration efficiency (99.996%) and a relatively low pressure drop (128.7 Pa) at a face velocity of 5.3 cm/s and a high antibacterial activity

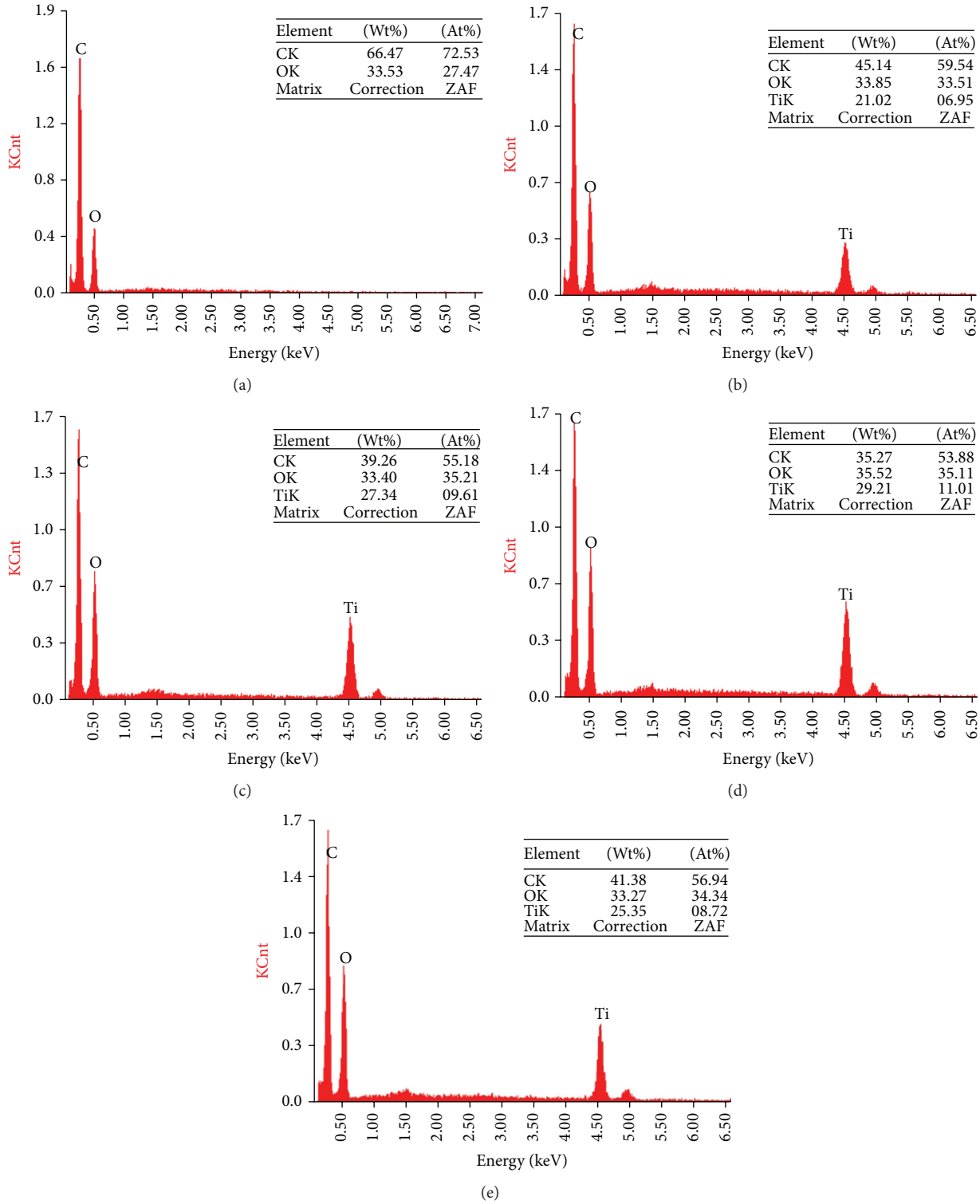

FIGURE 13: SEM-EDX spectra of the PLA/TiO_2 fibrous membranes after exposure under visible light for 30 days: (a) FM1, (b) FM2, (c) FM3, (d) FM4, and (e) FM5. The inset tables are the corresponding atomic ratio and weight ratio of the detected elements.

of 99.5%. This study provided a versatile approach to further design and develop multifunctional filters for respiratory protection, indoor air purification, and other filtration applications.

Conflict of Interests

The authors declare that there is no conflict of interests regarding the publication of this paper.

Acknowledgments

This study is supported by the Nanotechnology Special Project of the Suzhou Science and Technology Program Project (ZXG2012043), the Second-Phase Priority Academic Program Development of Jiangsu Higher Education Institutions (PAPD), the Graduate Student Innovation Project of Jiangsu Province (KYLX15_1245), and the Collaborative Innovation Institute of Research New Textile Materials of the Nan Tong Da Sheng Group (CP42014001).

References

[1] V. Thavasi, G. Singh, and S. Ramakrishna, "Electrospun nanofibers in energy and environmental applications," *Energy and Environmental Science*, vol. 1, no. 2, pp. 205–221, 2008.

[2] K. Yoon, B. S. Hsiao, and B. Chu, "Functional nanofibers for environmental applications," *Journal of Materials Chemistry*, vol. 18, no. 44, pp. 5326–5334, 2008.

[3] O. Yildiz and P. D. Bradford, "Aligned carbon nanotube sheet high efficiency particulate air filters," *Carbon*, vol. 64, pp. 295–304, 2013.

[4] C. Liu, P.-C. Hsu, H. Lee et al., "Transparent air filter for high-efficiency $PM_{2.5}$ capture," *Nature Communications*, vol. 6, article 6205, 2015.

[5] A. Vanangamudi, S. Hamzah, and G. Singh, "Synthesis of hybrid hydrophobic composite air filtration membranes for antibacterial activity and chemical detoxification with high particulate filtration efficiency (PFE)," *Chemical Engineering Journal*, vol. 260, pp. 801–808, 2015.

[6] S. Rodríguez, X. Querol, A. Alastuey et al., "Comparative PM10–PM2.5 source contribution study at rural, urban and industrial sites during PM episodes in Eastern Spain," *Science of the Total Environment*, vol. 328, no. 1–3, pp. 95–113, 2004.

[7] X. Li, N. Wang, G. Fan et al., "Electreted polyetherimide–silica fibrous membranes for enhanced filtration of fine particles," *Journal of Colloid and Interface Science*, vol. 439, pp. 12–20, 2015.

[8] C.-H. Hung and W. W.-F. Leung, "Filtration of nano-aerosol using nanofiber filter under low Peclet number and transitional flow regime," *Separation and Purification Technology*, vol. 79, no. 1, pp. 34–42, 2011.

[9] A. Joubert, J. C. Laborde, L. Bouilloux, S. Chazelet, and D. Thomas, "Modelling the pressure drop across HEPA filters during cake filtration in the presence of humidity," *Chemical Engineering Journal*, vol. 166, no. 2, pp. 616–623, 2011.

[10] S. Kaur, S. Sundarrajan, D. Rana, T. Matsuura, and S. Ramakrishna, "Influence of electrospun fiber size on the separation efficiency of thin film nanofiltration composite membrane," *Journal of Membrane Science*, vol. 392-393, pp. 101–111, 2012.

[11] R. S. Barhate and S. Ramakrishna, "Nanofibrous filtering media: filtration problems and solutions from tiny materials," *Journal of Membrane Science*, vol. 296, no. 1-2, pp. 1–8, 2007.

[12] R. Gopal, S. Kaur, Z. Ma, C. Chan, S. Ramakrishna, and T. Matsuura, "Electrospun nanofibrous filtration membrane," *Journal of Membrane Science*, vol. 281, no. 1-2, pp. 581–586, 2006.

[13] D. Li and Y. Xia, "Electrospinning of nanofibers: reinventing the wheel?" *Advanced Materials*, vol. 16, no. 14, pp. 1151–1170, 2004.

[14] Z.-W. Ma, M. Kotaki, and S. Ramakrishna, "Surface modified nonwoven polysulphone (PSU) fiber mesh by electrospinning: a novel affinity membrane," *Journal of Membrane Science*, vol. 272, no. 1-2, pp. 179–187, 2006.

[15] X. Wang, B. Ding, G. Sun, M. Wang, and J. Yu, "Electrospinning/netting: a strategy for the fabrication of three-dimensional polymer nano-fiber/nets," *Progress in Materials Science*, vol. 58, no. 8, pp. 1173–1243, 2013.

[16] N. Wang, X. Wang, B. Ding, J. Yu, and G. Sun, "Tunable fabrication of three-dimensional polyamide-66 nano-fiber/nets for high efficiency fine particulate filtration," *Journal of Materials Chemistry*, vol. 22, no. 4, pp. 1445–1452, 2012.

[17] L. Huang, J. T. Arena, S. S. Manickam, X. Jiang, B. G. Willis, and J. R. McCutcheon, "Improved mechanical properties and hydrophilicity of electrospun nanofiber membranes for filtration applications by dopamine modification," *Journal of Membrane Science*, vol. 460, pp. 241–249, 2014.

[18] S. Zhang, W. S. Shim, and J. Kim, "Design of ultra-fine nonwovens via electrospinning of Nylon 6: spinning parameters and filtration efficiency," *Materials and Design*, vol. 30, no. 9, pp. 3659–3666, 2009.

[19] A. Patanaik, V. Jacobs, and R. D. Anandjiwala, "Performance evaluation of electrospun nanofibrous membrane," *Journal of Membrane Science*, vol. 352, no. 1-2, pp. 136–142, 2010.

[20] Y. Wang, W. Li, Y. Xia, X. Jiao, and D. Chen, "Electrospun flexible self-standing γ-alumina fibrous membranes and their potential as high-efficiency fine particulate filtration media," *Journal of Materials Chemistry A*, vol. 2, no. 36, pp. 15124–15131, 2014.

[21] P. Li, C. Wang, Y. Zhang, and F. Wei, "Air filtration in the free molecular flow regime: a review of high-efficiency particulate air filters based on carbon nanotubes," *Small*, vol. 10, no. 22, pp. 4553–4561, 2014.

[22] P. Li, Y. Zong, Y. Zhang et al., "In situ fabrication of depth-type hierarchical CNT/quartz fiber filters for high efficiency filtration of sub-micron aerosols and high water repellency," *Nanoscale*, vol. 5, no. 8, pp. 3367–3372, 2013.

[23] Z. Wang and Z. Pan, "Preparation of hierarchical structured nano-sized/porous poly(lactic acid) composite fibrous membranes for air filtration," *Applied Surface Science*, vol. 356, pp. 1168–1179, 2015.

[24] Y. Yang, S. Zhang, X. Zhao, J. Yu, and B. Ding, "Sandwich structured polyamide-6/polyacrylonitrile nanonets/bead-on-string composite membrane for effective air filtration," *Separation and Purification Technology*, vol. 152, pp. 14–22, 2015.

[25] N. Wang, Y. Si, N. Wang et al., "Multilevel structured polyacrylonitrile/silica nanofibrous membranes for high-performance air filtration," *Separation and Purification Technology*, vol. 126, pp. 44–51, 2014.

[26] Z. Wang, C. Zhao, and Z. Pan, "Porous bead-on-string poly(lactic acid) fibrous membranes for air filtration," *Journal of Colloid and Interface Science*, vol. 441, pp. 121–129, 2015.

[27] W. S. Lee, Y.-S. Park, and Y.-K. Cho, "Significantly enhanced antibacterial activity of TiO_2 nanofibers with hierarchical nanostructures and controlled crystallinity," *Analyst*, vol. 140, no. 2, pp. 616–622, 2015.

[28] S.-Y. Ryu, J. W. Chung, and S.-Y. Kwak, "Dependence of photocatalytic and antimicrobial activity of electrospun polymeric nanofiber composites on the positioning of Ag–TiO_2 nanoparticles," *Composites Science and Technology*, vol. 117, pp. 9–17, 2015.

[29] X. Chen and S. S. Mao, "Titanium dioxide nanomaterials: synthesis, properties, modifications and applications," *Chemical Reviews*, vol. 107, no. 7, pp. 2891–2959, 2007.

[30] H. R. Pant, D. R. Pandeya, K. T. Nam, W.-I. Baek, S. T. Hong, and H. Y. Kim, "Photocatalytic and antibacterial properties of a TiO_2/nylon-6 electrospun nanocomposite mat containing silver nanoparticles," *Journal of Hazardous Materials*, vol. 189, no. 1-2, pp. 465–471, 2011.

[31] I. Chauhan and P. Mohanty, "In situ decoration of TiO_2 nanoparticles on the surface of cellulose fibers and study of their photocatalytic and antibacterial activities," *Cellulose*, vol. 22, no. 1, pp. 507–519, 2015.

[32] J. Lin, B. Ding, Y. Jianyong, and Y. Hsieh, "Direct fabrication of highly nanoporous polystyrene fibers via electrospinning," *Applied Materials and Interfaces*, vol. 2, no. 2, pp. 521–528, 2010.

[33] P. Dayal, J. Liu, S. Kumar, and T. Kyu, "Experimental and theoretical investigations of porous structure formation in electrospun fibers," *Macromolecules*, vol. 40, no. 21, pp. 7689–7694, 2007.

[34] C. L. Casper, J. S. Stephens, N. G. Tassi, D. B. Chase, and J. F. Rabolt, "Controlling surface morphology of electrospun polystyrene fibers: effect of humidity and molecular weight in the electrospinning process," *Macromolecules*, vol. 37, no. 2, pp. 573–578, 2004.

[35] J. Lin, B. Ding, J. Yang, J. Yu, and G. Sun, "Subtle regulation of the micro- and nanostructures of electrospun polystyrene fibers and their application in oil absorption," *Nanoscale*, vol. 4, no. 1, pp. 176–182, 2012.

[36] B. Ding, J. Lin, X. Wang, J. Yu, J. Yang, and Y. Cai, "Investigation of silica nanoparticle distribution in nanoporous polystyrene fibers," *Soft Matter*, vol. 7, no. 18, pp. 8376–8383, 2011.

[37] J. Yu and J. Ran, "Facile preparation and enhanced photocatalytic H_2-production activity of $Cu(OH)_2$ cluster modified TiO_2," *Energy and Environmental Science*, vol. 4, no. 4, pp. 1364–1371, 2011.

[38] J. G. Yu, Y. R. Su, and B. Cheng, "Template-free fabrication and enhanced photocatalytic activity of hierarchical macro-/mesoporous titania," *Advanced Functional Materials*, vol. 17, no. 12, pp. 1984–1990, 2007.

[39] J. Lin, F. Tian, Y. Shang, F. Wang, B. Ding, and J. Yu, "Facile control of intra-fiber porosity and inter-fiber voids in electrospun fibers for selective adsorption," *Nanoscale*, vol. 4, no. 17, pp. 5316–5320, 2012.